

## Production, ionization and redistribution of O<sub>2</sub> in Saturn's ring atmosphere

R.E. Johnson<sup>a,b,\*</sup>, J.G. Luhmann<sup>c</sup>, R.L. Tokar<sup>d</sup>, M. Bouhram<sup>e</sup>, J.J. Berthelier<sup>f</sup>, E.C. Sittler<sup>f</sup>,  
J.F. Cooper<sup>f</sup>, T.W. Hill<sup>g</sup>, H.T. Smith<sup>a</sup>, M. Michael<sup>a,e</sup>, M. Liu<sup>a</sup>, F.J. Cray<sup>h</sup>, D.T. Young<sup>h</sup>

<sup>a</sup> *Engineering Physics, University of Virginia, Charlottesville, VA 22904, USA*

<sup>b</sup> *Physics Department, New York University, NY 10003, USA*

<sup>c</sup> *Space Sciences Laboratory, University of California Berkeley, CA 94720, USA*

<sup>d</sup> *Space and Atmospheric Science Group, Los Alamos National Laboratory, Los Alamos, NM 87545, USA*

<sup>e</sup> *Centre d'étude des Environnements Terrestre et Planétaires, Observatoire de St. Maur, 94107 St. Maur, France*

<sup>f</sup> *Goddard Space Flight Center, Greenbelt, MD 20771, USA*

<sup>g</sup> *Department of Physics and Astronomy, Rice University, Houston, TX 77251, USA*

<sup>h</sup> *Southwest Research Institute, 9VTT Information Technology, 02044, San Antonio, TX 78238, USA*

Received 30 April 2005; revised 9 August 2005

Available online 16 November 2005

### Abstract

Molecular oxygen produced by the decomposition of icy surfaces is ubiquitous in Saturn's magnetosphere. A model is described for the toroidal O<sub>2</sub> atmosphere indicated by the detection of O<sub>2</sub><sup>+</sup> and O<sup>+</sup> over the main rings. The O<sub>2</sub> ring atmosphere is produced primarily by UV photon-induced decomposition of ice on the sunlit side of the ring. Because O<sub>2</sub> has a long lifetime and interacts frequently with the ring particles, equivalent columns of O<sub>2</sub> exist above and below the ring plane with the scale height determined by the local ring temperature. Energetic particles also decompose ice, but estimates of their contribution over the main rings appear to be very low. In steady state, the O<sub>2</sub> column density over the rings also depends on the relative efficiency of hydrogen to oxygen loss from the ring/atmosphere system with oxygen being recycled on the grain surfaces. Unlike the neutral density, the ion densities can differ on the sunlit and shaded sides due to differences in the ionization rate, the quenching of ions by the interaction with the ring particles, and the northward shift of the magnetic equator relative to the ring plane. Although O<sup>+</sup> is produced with a significant excess energy, O<sub>2</sub><sup>+</sup> is not. Therefore, O<sub>2</sub><sup>+</sup> should mirror well below those altitudes at which ions were detected. However, scattering by ion–molecule collisions results in much larger mirror altitudes, in ion temperatures that go through a minimum over the B-ring, and in the redistribution of both molecular hydrogen and oxygen throughout the magnetosphere. The proposed model is used to describe the measured oxygen ion densities in Saturn's toroidal ring atmosphere and its hydrogen content. The oxygen ion densities over the B-ring appear to require either significant levels of UV light scattering or ion transmission through the ring plane.

© 2005 Elsevier Inc. All rights reserved.

*Keywords:* Saturn; Magnetosphere; Atmosphere; Rings

### 1. Introduction

The Cassini Plasma Spectrometer (CAPS) (Young et al., 2005) and the Ion Neutral Mass Spectrometer (INMS) (Waite et al., 2005) detected thermal O<sup>+</sup> and O<sub>2</sub><sup>+</sup> over Saturn's main ring shortly after Cassini's orbit insertion. CAPS detected the O<sup>+</sup> and O<sub>2</sub><sup>+</sup> on July 1, 2004 over a radial distance range of 1.79 to 2.10 R<sub>S</sub> (Fig. 1) and INMS detected the O<sup>+</sup> and O<sub>2</sub><sup>+</sup> from

~2.12–2.2 R<sub>S</sub>, where R<sub>S</sub> (~60,300 km) is a Saturn radius. Both sets of measurements occurred north of the ring plane with the sun 23.6° south of the ring plane. Tokar et al. (2005) showed that O<sub>2</sub><sup>+</sup> extends into the magnetosphere inside the G-ring and energetic O<sub>2</sub><sup>+</sup> was observed throughout the magnetosphere (Krimigis et al., 2005). Based on these measurements, O<sub>2</sub><sup>+</sup> is present in densities greater than expected in all regions of Saturn's magnetosphere. Therefore, in addition to the hydrogen (Shemansky and Hall, 1992), OH (Jurac et al., 2002) and nitrogen toroidal atmospheres (Smith et al., 2004), molecular oxygen torii are important components of Saturn's magnetosphere.

\* Corresponding author. Fax: +1 434 924 1353.

E-mail address: [rej@virginia.edu](mailto:rej@virginia.edu) (R.E. Johnson).

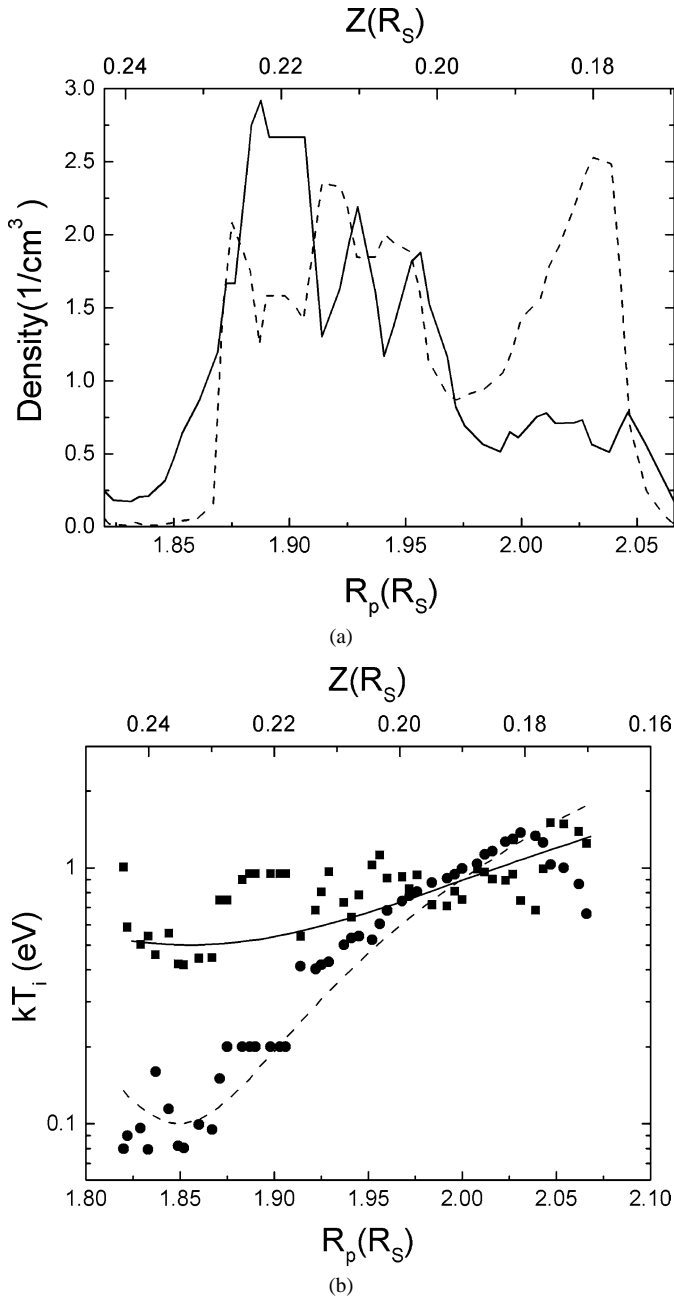


Fig. 1.  $O_2^+$  and  $O^+$  densities and temperatures vs distance along the equatorial plane  $R_p$  in  $R_S$ : the  $O^+$  can contain some  $OH^+$  [adapted from Tokar et al. (2005)]. (a)  $O^+$  (solid) and  $O_2^+$  (dashed) densities at the spacecraft altitude measured by CAPS. Over the B-ring the ion density was less than the electron density as determined by the plasma wave experiments. (b) Measured ion temperatures for  $O^+$  (squares) and  $O_2^+$  (dots) vs  $R_p$ . Lines are the corresponding model temperatures  $E_i^* + E_p$ .

A toroidal ring atmosphere consisting of water molecules produced by meteoroid impacts (Ip, 1984; Pospieszalska and Johnson, 1991) or photosputtering (Carlson, 1980) had been predicted and the resulting plasma was thought to account for the transient ‘spokes’ seen over the main rings by Voyager (Grun et al., 1983). Ip (1995) proposed that the gas-phase photo-dissociation of the ejected water molecules produced fragments that resulted in a tenuous  $O_2$  torus ( $\sim 10^3 \text{ cm}^{-3}$ ) and that  $O_2^+$  was present in the inner magnetosphere (Ip, 2000,

2005). Whereas water molecules and their fragments stick or react on grains with nearly unit efficiency, any  $O_2$  that is formed does not. Therefore,  $O_2$  can accumulate over the rings, similar to its accumulation over the surfaces of Europa and Ganymede (Shematovich et al., 2005). Although  $O_2$  can be produced from dissociated water fragments by gas-phase (Yung and McElroy, 1977) and surface (Ip, 1995) processes, at Europa and Ganymede  $O_2$  is a signature of the decomposition of ice by incident energetic ions and electrons, a process often called radiolysis (Johnson et al., 2003, 2004). Decomposition refers to the break down of water into  $O_2$  and  $H_2$ . Therefore, like the observation of an ‘ozone’ feature on Dione and Rhea (Noll et al., 1997), the observation of molecular oxygen ions in Saturn’s magnetosphere is a marker for radiation-induced decomposition of the ice grains and the icy bodies that orbit within the magnetosphere. Unlike at Europa and Ganymede, the energetic ion and electron flux onto the main rings is small (Simpson et al., 1980; Cooper, 1983; Chenette et al., 1980; Young et al., 2005; Krimigis et al., 2005). Therefore, we propose that UV photons decompose ice by photolysis, producing a toroidal  $O_2$  atmosphere over the rings that is more robust than that predicted.

Because the neutrals in the oxygen torus are confined to a region closer to the ring plane than where CAPS detected ions, in our model we describe the heating of the freshly formed ions by ion-molecule collisions. We also account for the effect of the northward displacement of the magnetic equator. Although the Cassini Orbiter will not fly over the main rings again during its prime mission, it will pass reasonably close ( $\sim 2.5 R_S$ ) to the edge of the main rings. Because the oxygen from the toroidal ring atmosphere can populate this region and more distant regions of the magnetosphere, a good model of this atmosphere will be needed in order to interpret Cassini plasma data.

## 2. Oxygen atmosphere

Oxygen atmospheres were predicted to be present on the icy satellites of Jupiter produced by the photolysis of water vapor (Yung and McElroy, 1977) and due to the radiolytic decomposition of ice (Johnson et al., 1982; Johnson, 1990). Thin oxygen atmospheres were eventually detected (Hall et al., 1995; McGrath et al., 2004) that were formed, not by photolysis in the gas-phase, but by the radiolytic decomposition of ice by the energetic charged particle flux (Johnson et al., 2004). Although decomposition of ice also produces molecular hydrogen, it readily escapes Europa’s gravitational field while molecular oxygen does not. Therefore, Europa creates a significant hydrogen torus in Jupiter’s magnetosphere (Shematovich et al., 2005) but not a very robust molecular oxygen torus (Burger and Johnson, 2004; Hansen et al., 2005). Unlike the jovian icy satellites, the icy Saturn satellites and ring particles have relatively small gravitational effects. Therefore, radiation-induced decomposition of these icy bodies *directly* populates Saturn’s magnetosphere, forming toroidal oxygen atmospheres in which the molecules co-orbit with these sources (e.g., Ip, 2005). Although  $O_2$  is not the dominant ejecta produced by the incident radiation, it does not condense at the surface temperatures in

Saturn's system and has an ionization potential smaller than the other water products. Therefore, decomposition of ice is the principal source of O<sub>2</sub> in Saturn's magnetosphere and O<sub>2</sub><sup>+</sup> is a relatively stable species throughout the magnetosphere.

That electronic excitations in ice can decompose water molecules has been known for over 50 years (Johnson et al., 2003). Brown et al. (1982) revived interest in this process by measuring the decomposition induced by energetic ions like those in Jupiter's magnetosphere, a process often referred to as radiolysis (Johnson and Quickenden, 1997). Subsequently, it was shown that O<sub>2</sub> is also produced from ice by Lyman- $\alpha$  photons (Westley et al., 1995) and low energy (6–100 eV) electrons (Sieger et al., 1998). In these laboratory experiments, the formation of O<sub>2</sub> follows the prompt loss of hydrogen from ice. Therefore, after a small initial dose, the irradiated layer of the ice becomes slightly oxidizing, which favors the formation of O<sub>2</sub> and oxygen-rich species in the icy surface (Johnson et al., 2003).

Although the fluxes are very low, cosmic ray and energetic particles at MeV to GeV energies are the dominant sources for ionization in the main ring particles. Any O<sub>2</sub> produced in the bulk by penetrating radiation can, in principal, be released by collisions and meteoroid bombardment. However, the energy deposition rate  $\sim 0.3$  GeV/cm<sup>2</sup>/s based on Pioneer 11 data (Cooper et al., 1985) gives an upper limit to the steady state cosmic ray production of O<sub>2</sub> (Cooper et al., 2001; Johnson et al., 2003) that is an order of magnitude smaller than UV-induced decomposition. Energetic magnetospheric particles interact at rapidly declining flux levels with icy bodies at the outer edge of the A ring (Simpson et al., 1980; Eviatar et al., 1983; Paranicas et al., 1997) and with bodies in the F and G rings at higher flux levels (Maurice et al., 2004), partially accounting for O<sub>2</sub><sup>+</sup> observations inside the G ring (Tokar et al., 2005). However, the low plasma temperatures and densities over the main rings suggest that photolysis of ice is the principal source of O<sub>2</sub> gas above the main rings.

The yield for the production of O<sub>2</sub> from ice by Lyman- $\alpha$  photons was measured by Westley et al. (1995) (Table 1). Using the Lyman- $\alpha$  flux at Saturn, the source rate for production of O<sub>2</sub> from ice is:  $S_{O_2} \cong 10^6$  O<sub>2</sub>/cm<sup>2</sup>/s (Johnson et al., 2003). We have assumed that the yield varies nearly inversely on the incident angle (e.g., Johnson et al., 2003) roughly canceling the projection effect on the ring plane. Since photons with lower energies can also produce molecular O<sub>2</sub> from ice ( $\sim 6$  eV; Orlando and Grieves, 2005; Orlando and Sieger, 2003), this is a *lower limit* to  $S_{O_2}$ . Additional measurements are in progress to more carefully examine these issues.

Using available G-values (Johnson et al., 2003; Cooper et al., 2001), the energetic secondary particles produced from the rings by galactic cosmic rays, and observed by Pioneer (Simpson et al., 1980; Maurice et al., 2004), produce more than an order of magnitude less O<sub>2</sub> than does the flux of inner radiation belt ions impacting the edge of the main rings. Water vapor produced by meteoroid impacts or UV desorption, or water coming from regions outside the rings is also photo-dissociated by UV radiation. However, the resulting radicals rapidly stick to the ring particle surfaces. Therefore, any contribution such rad-

Table 1  
Data for ring atmosphere

Yield (100 K) (Lyman- $\alpha$ )	0.0003O <sub>2</sub> /photon
$S_{O_2}$ ( $S_{H_2}/2$ )	$>10^6$ O <sub>2</sub> /cm <sup>2</sup> /s
$v_o$	$18.5(1.85R_S/R)^{1/2}$ km/s
$\tau_b$ ( $\approx \pi R/v_o$ )	$1.1 \times 10^4$ s ( $2R_S$ )
$\tau_{co}$	$3.9 \times 10^4$ s
$\langle v_T \rangle = (8kT/\pi m)^{1/2}$	0.26 km/s for $T = 100$ K
$H_{O_2}$ ( $\approx R\langle v_T \rangle/v_o$ ) ( $H_{H_2}/4$ )	1600 km ( $2R_S$ )
$\tau_{io}$ (O <sub>2</sub> + $h\nu \rightarrow$ O <sub>2</sub> <sup>+</sup> + $e$ )	$1.1 \times 10^8$ s <sup>a</sup>
$\tau_{ih}$ (H <sub>2</sub> + $h\nu \rightarrow$ H <sub>2</sub> <sup>+</sup> + $e$ )	$1.0 \times 10^9$ s <sup>a</sup>
$\tau_{ido}$ (O <sub>2</sub> + $h\nu \rightarrow$ O + O <sup>+</sup> + $e$ )	$4.0 \times 10^8$ s <sup>a</sup> [ $\sim 0.5$ eV] <sup>b</sup>
$\tau_{idh}$ (H <sub>2</sub> + $h\nu \rightarrow$ H + H <sup>+</sup> + $e$ )	$6.2 \times 10^9$ s <sup>a</sup>
$\tau_{do}$ (O <sub>2</sub> + $h\nu \rightarrow$ O + O)	$1.7 \times 10^7$ s [ $0.8$ eV] <sup>a</sup>
$\tau_{dh}$ (H <sub>2</sub> + $h\nu \rightarrow$ H + H)	$6.7 \times 10^7$ s [ $2.5$ eV] <sup>a</sup>
$\tau'_{O_2} = [\tau_{do}^{-1} + \tau_{ido}^{-1} + \tau_{io}^{-1}]^{-1}$	$1.4 \times 10^7$ s <sup>a</sup>
$\tau'_{H_2} = [\tau_{dh}^{-1} + \tau_{idh}^{-1} + \tau_{ih}^{-1}]^{-1}$	$3.8 \times 10^8$ s <sup>a</sup>
<sup>c</sup> $\tau_{bi}$	$\sim 2.0 \times 10^4$ s
<sup>d</sup> $\tau_{ci} (k_{io}n_o)^{-1}$	$(0.7 \times 10^4/c_e)$ s (outer edge of B-ring)
<sup>e</sup> $\tau_s$	$3.8 \times 10^4$ s

<sup>a</sup> Photoionization and dissociation [mean excess energy of O or H]: Huebner et al. (1992) average of quiet Sun and active Sun. Primes: upper bounds to lifetimes (e.g., ignore  $c_e$ ).

<sup>b</sup> Luna et al. (2005) [mean excess energy of O<sup>+</sup>].

<sup>c</sup> Average bounce time for O<sub>2</sub><sup>+</sup> produced near ring plane, mirroring and returning (Luhmann et al., 2005).

<sup>d</sup> Time for collision of an O<sub>2</sub><sup>+</sup> ion with an O<sub>2</sub> near the ring plane obtained using lower limit to the O<sub>2</sub> density,  $n_o$ , where  $c_e$ , is the enhancement factor discussed in text ( $\gtrsim 10$ ). The reaction rate is:  $k_{io} = \langle \sigma_{io} v \rangle = 2\pi[\alpha(z_e)^2/m]^{1/2} = 7.4 \times 10^{-10}$  cm<sup>3</sup>/s where  $\sigma_{io}$  is the Langevin cross section and  $\alpha$  the polarizability of O<sub>2</sub>.

<sup>e</sup>  $\tau_s$  Saturn rotation period (ion co-rotation time).

icals might make to  $S_{O_2}$  would also be by UV photon-induced desorption from the surfaces of the ring particles. Since most of the solar UV is absorbed by the ring particles, and not in an ambient gas, in the following calculations we use the Lyman- $\alpha$ -induced production rate as a *lower limit* to the O<sub>2</sub> source rate.

Since the ring particles are not pure water ice, we write the net source rate of O<sub>2</sub> from the sunlit side of the icy rings as  $[c_{ice}(1-f)S_{O_2}]$ . Here  $f$  is the fraction of the sunlight transmitted through the rings,  $f = \exp(-\xi/\cos\theta)$ , where  $\xi$  is the optical thickness of the ring,  $\theta$  is the angle of incidence of solar UV flux to the ring plane, and  $c_{ice}$  is the ice fraction in the surface of the attenuating particles. O<sub>2</sub> is ejected with a slightly non-thermal energy distribution  $[\sim U/(E+U)^2$  with  $U = 0.015$  eV; Johnson, 1990]. However, over the A- and B-rings the ejected O<sub>2</sub> has a high probability of adsorbing onto and desorbing from a ring particle in one bounce period,  $\tau_b$ , ( $\sim 10^4$  s), which is about half the orbital period for a neutral (Table 1). Since the photo-dissociation lifetime,  $\tau_{do}$  ( $\sim 2 \times 10^7$  s), is three orders of magnitude larger than  $\tau_b$  and the residence time (<seconds) of an O<sub>2</sub> molecule on a grain is much shorter than  $\tau_b$ , the O<sub>2</sub> atmosphere is thermally accommodated to ring particles. Therefore, the gas-phase O<sub>2</sub> will not be hot as assumed by (Ip, 1995) but will have a mean energy  $\sim 2kT$ , where  $T$  is average surface temperature of ring particles ( $\sim 80$ – $100$  K).

Since an O<sub>2</sub> molecule is, on the average, absorbed by the ring particles and re-emitted randomly  $\sim 10^3$  times during its

lifetime, the O<sub>2</sub> atmosphere populates *both the shadowed and sunlit* sides of the rings. Using the source rate for the sunlit side [ $c_{\text{ice}}S_{\text{O}_2}(1-f)$ ] and an O<sub>2</sub> lifetime,  $\tau_{\text{O}_2}$ , then the average neutral column densities on either side of the rings is

$$N_{\text{O}_2}(R) \approx c_{\text{ice}}S_{\text{O}_2}\tau_{\text{O}_2}[(1-f)/(1+f)]. \quad (1)$$

The quantity  $[(1+f)/\tau_{\text{O}_2}]$  in Eq. (1) is the average photo-destruction rate of O<sub>2</sub> for the sunlit and shaded sides of the ring plane. Because O from photo-dissociation of O<sub>2</sub> rapidly adsorb onto ring particle surfaces, the ring-atmosphere is primarily molecular. Based on the values of  $f$  in Table 1, and ignoring differences in  $c_{\text{ice}}$ , this atmosphere is most dense over the B-ring and least dense over the Cassini gap and C-ring. These densities are somewhat insensitive to the solar conditions because both the source and loss processes depend on the UV flux.

The escape probability for thermal O<sub>2</sub> from the region of the rings is small so that the vertical distribution can be roughly described by

$$n_{\text{O}_2}(z, R) \approx n_o(R) \exp[-(z/H_{\text{O}_2})^2], \quad z \ll R_S, \quad (2)$$

where  $z$  is the height above the ring plane and  $R$  is the distance from Saturn. The density in the ring plane,  $n_o$ , is  $\sim[(2/\pi^{1/2})(N_{\text{O}_2}/H_{\text{O}_2})]$ , and the centrifugal scale height for neutrals is  $H_{\text{O}_2} \approx R\langle v_T \rangle/v_o(R)$ , where  $\langle v_T \rangle [= (8kT/\pi m)^{1/2}]$  and  $v_o(R)$  is the Keplerian orbital speed (Johnson, 1990; Ip, 1995). For an average ring particle surface temperature  $\sim 100$  K,  $\langle v_T \rangle$  is 0.26 km/s for O<sub>2</sub>, in which case  $H_{\text{O}_2} \approx 1600$  km at  $2R_S$  and varies roughly as  $R^{-3/2}$ . Therefore, in the absence of additional heating processes, the atmosphere lies below the magnetic equator, located  $\sim 2500$  km north of the ring plane, and well below the spacecraft altitudes at which CAPS detected oxygen ions (0.15–0.25  $R_S$  corresponding to  $\sim 9000$ –15,000 km).

Using an O<sub>2</sub> lifetime determined by ionization and dissociation [ $\tau_{\text{O}_2} \approx \tau'_{\text{O}_2}$ ; Table 1], lower limits to  $N_{\text{O}_2}$  can be obtained (Table 2). Such estimates ignore edge effects due to the high inclination of the Sun during Cassini SOI, and radial transport. These would smooth over the variations in the optical thickness and density, particularly at the Cassini gap which is only  $\sim 3$  scale heights wide. Recycling of O<sub>2</sub><sup>+</sup>, O<sup>+</sup> and O on the grain surfaces increases  $\tau_{\text{O}_2}$  as shown below. Since the ring atmosphere was not directly detected, ion production and loss are first described.

Table 2  
Ring atmosphere parameters: solar zenith angle  $\sim 66^\circ$

Rings (extent)	A (2.27–2.03 $R_S$ )	Cassini (2.03–1.95 $R_S$ )	B (1.95–1.53 $R_S$ )
Area (10 <sup>20</sup> cm <sup>2</sup> )	0.55	0.18	0.97
$\xi(f)^a$	0.6 (0.23)	0.12 (0.74)	1.6 (0.02)
$[1-f]/[1+f](xf)^b$	0.63 (0.14)	0.15 (0.11)	0.96 (0.019)
$N_{\text{O}_2}$ (10 <sup>13</sup> O <sub>2</sub> /cm <sup>2</sup> ) <sup>c</sup>	$>0.4c_e c_{\text{ice}}$	$>0.1c_e c_{\text{ice}}$	$>0.7c_e c_{\text{ice}}$

<sup>a</sup> Rough average optical depth,  $\xi$ , and, brackets, transmission factor,  $f$ , using  $66^\circ$  zenith angle.

<sup>b</sup> Factor in Eq. (1); brackets: factor in Eq. (4b) for  $f_i = 0$ .

<sup>c</sup> O<sub>2</sub> column density using Eq. (1) with  $\tau_{\text{O}_2} = c_e \tau'_{\text{O}_2}$  at mean solar activity where  $c_e$  is the ratio of the escape efficiency of H relative to O and  $c_{\text{ice}}$  is the fraction of the ring particle composition that is ice: this is lower for the particles in the Cassini division and the C-ring than either the A- or B-rings.

### 3. Ion column densities

Although the O<sub>2</sub> densities are assumed to be similar on the sunlit and shaded sides of the ring plane, the ion densities are not. Photo-ionization of O<sub>2</sub>, which produces both O<sub>2</sub><sup>+</sup> and O<sup>+</sup> (Table 1), is reduced on the shaded side by the optical thickness of the rings. Unlike O<sub>2</sub> the ion lifetimes are short due to collisions with ring particles, leading to neutralization or surface reactions. The newly formed ions attempt to move between mirror points that are symmetric with respect to the magnetic equator, which is shifted north of the ring plane, affecting the asymmetry.

The observed ions have small gyro-radii,  $r_g$  ( $< 0.1$  km for O<sub>2</sub><sup>+</sup>) and have a probability,  $f_i$ , for surviving passage through the rings. The column densities on the sunlit,  $N_{\text{si}}$ , and shaded,  $N_{\text{shi}}$ , sides of the rings can be described by two rate equations:

$$dN_{\text{si}}/dt \approx N_{\text{O}_2}/\tau_i - N_{\text{si}}/\tau_{\text{si}} + N_{\text{shi}}f_i/\tau_{\text{si}}, \quad (3a)$$

$$dN_{\text{shi}}/dt \approx N_{\text{O}_2}f/\tau_i + N_{\text{si}}f_i/\tau_{\text{shi}} - N_{\text{shi}}/\tau_{\text{shi}}. \quad (3b)$$

The first terms describe the ionization of the neutrals where  $\tau_i$  is the ion formation time, either  $\tau_{\text{io}}$  for O<sub>2</sub><sup>+</sup> production or  $\tau_{\text{id}}$  for O<sup>+</sup> production. Values are given in Table 1. The second and third terms on the right are due to transport across the ring plane, where  $\tau_{\text{si}}$  and  $\tau_{\text{shi}}$  are the times spent on either side before crossing the ring plane. In this model, ion loss is assumed to occur primarily by interaction with the ring particles through  $(1-f_i)$ . Ignoring the dipole offset, then  $\tau_{\text{si}} \sim \tau_{\text{shi}} \sim \tau_{\text{bi}}$ , where  $\tau_{\text{bi}}$  is the average bounce time, about half the time between mirror points (e.g., Luhmann et al., 2005).

Solving Eqs. (3), the steady state column densities are

$$N_{\text{si}} \approx N_{\text{O}_2}(\tau_{\text{bi}}/\tau_i)(1+ff_i)/(1-f_i^2), \quad (4a)$$

$$N_{\text{shi}} \approx N_{\text{O}_2}(\tau_{\text{bi}}/\tau_i)(f_i+f)/(1-f_i^2), \quad (4b)$$

where, again,  $f$  is the fraction of light penetrating the rings. The singular behavior at  $f_i = 1$ , resulting from our neglect of loss processes other than ring absorption, is not a problem because in practice  $f_i < 1$  over the main rings. Inserting  $N_{\text{O}_2}$  from Eq. (1), the ion column densities above and below the ring plane are proportional to the ratio of the lifetime for O<sub>2</sub> destruction to the ionization lifetime,  $[\tau_{\text{O}_2}/\tau_i]$ , which is, roughly, independent of solar conditions. In addition, if the ion transmission efficiency,  $f_i$ , and the ion bounce time,  $\tau_{\text{bi}}$ , are similar for O<sup>+</sup> and O<sub>2</sub><sup>+</sup>, then the ratio of the O<sup>+</sup> to O<sub>2</sub><sup>+</sup> column densities on either side of the ring plane is equal to the *branching ratio*

for ionization, which is  $\sim 0.24$ – $0.30$  depending on solar activity (Table 1).

The ratio of the steady state column densities is determined by the optical thickness of the rings to both ions and UV-photons:

$$N_{\text{shi}}/N_{\text{si}} \approx (f_i + f)/(1 + ff_i). \quad (5)$$

The ability of the ions to wend their way through the rings,  $f_i$ , is determined roughly by  $\xi$ , the ion's pitch angle and gyroradius, and, possibly, the charging of the ring particles. If all ions are absorbed on crossing the ring plane, then  $f_i = 0$  and the column density ratio is  $\sim f$ , the photon penetration efficiency. Ignoring scattered light, the oblique incidence [ $\cos^{-1}(\theta) = 2.5$  at SOI] causes  $f$  to be very small over the B-ring so the density ratio,  $\sim(f_i + f)$ , can be dominated by ion transmission. Note that, if  $f_i$  for ion transmission is also small, then the column density over the Cassini gap on the shaded side of ring would be *larger* than that over the B-ring, opposite to the neutral density. Scattered light and oblique incidence through the Cassini gap, allowing illumination of the gas above the A- and B-rings, can smooth over these differences. Since Cassini was also in Saturn's shadow during the CAPS measurement period, simulations will eventually be required.

#### 4. Dipole offset and ion-molecule collisions

The ion energy in the corotating frame is, roughly,  $E_i^* + E_p$ , where  $E_i^*$  is ion energy at formation and  $E_p$  is the pick-up gyro-energy,  $\sim m_i(v_{\text{co}} - v_o)^2/2$ .  $E_i^*$  is the initial thermal energy,  $E_i$ , plus the energy it attains due to formation off the equator. Whereas  $\text{O}^+$  is formed 'hot' ( $E_i \sim 0.5$  eV at peak), exhibiting a range of pitch angles and mirror altitudes, the newly formed  $\text{O}_2^+$  ( $E_i \sim 2$  kT) has pitch angles  $\sim \pi/2$ . Therefore, accounting for the off-set dipole,  $\text{O}_2^+$  will initially have northern mirror points in the vicinity of  $z_m \sim 0.08R_S \sim 5000$  km. This results in a vertical scale much larger than that for neutral  $\text{O}_2$ , but *well below* the region measured by CAPS ( $\sim 9000$ – $15,000$  km north). Therefore, the dipole offset alone cannot account for the CAPS measurements. The  $\text{O}_2^+$  ions must have been either scattered, heated or affected by electric fields prior to detection. Here we show that ion-molecule collisions alone can give mirror latitudes sufficiently large to account for the CAPS measurements.

Over the A- and B-rings, where the neutral density is large, the ion-molecule collision time ( $\tau_{\text{ci}}$ ), obtained using estimates of  $c_e$  below, is short compared to the ion bounce time,  $\tau_{\text{bi}}$  (Table 1). Therefore, newly formed ions can be scattered by  $\text{O}_2$  before they leave the formation region. After mirroring, these ions can again be scattered as they move obliquely through the neutral cloud. At these distances from Saturn, the relative collision speed is low, so that the ion and molecule can orbit each other before separating. The cross section for such a collision is determined by the polarizability of  $\text{O}_2$ . This results in a collision time,  $\tau_{\text{ci}}$ , that is independent of the relative velocity (Johnson, 1990; Table 1). For  $\text{O}_2^+ + \text{O}_2$  collisions, elastic scattering and charge exchange are indistinguishable. Therefore, the scattered

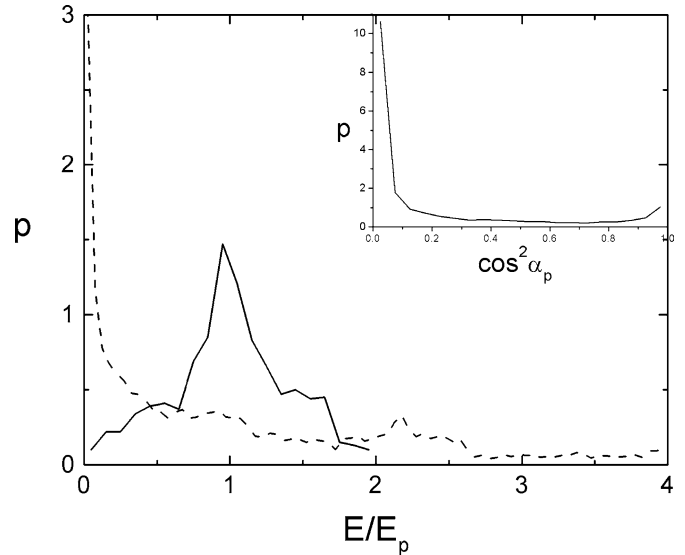


Fig. 2. Distribution function,  $p$ , of energies following an  $\text{O}_2^+ + \text{O}_2$  collision in which orbiting occurred. Exiting ion energies are given in the rotating frame (solid) and neutral energies in the Kepler orbit frame (dashed line). Both are given as a fraction of the pick-up gyro-energy,  $E_p$ . Note: these essentially define an ion/neutral 'temperature' which is of the size of  $(v_{\text{co}} - v_o)$  hence independent of  $R$ . (The insert shows the pitch angle distribution,  $p$ , as a function of  $\cos^2 \alpha_p$ ; average  $\cos^2 \alpha_p$  is 0.23; loss cone located at,  $\cos^2 \alpha_p \sim 0.8$  near the inner edge of the B-ring and  $\sim 0.95$  near the outer edge of the A-ring.)

ion attains a new velocity equal to the velocity of the center of mass in the inertial frame plus a velocity in a random direction that is equal to half the relative collision speed. For such collisions, it is seen in Fig. 2 that the scattered ions attain a broad distribution of energies in the rotating system, but with a 'thermal' energy about equal to the initial pick-up energy. Since the neutral  $\text{O}_2$  can also attain quite large energies, as indicated in Fig. 2, it can be scattered into regions outside of the main rings (Fig. 3), possibly accounting for the  $\text{O}_2^+$  detection just beyond the main rings by Tokar et al. (2005).

Because  $v_{\text{co}}$  and  $v_o$  are not very different over the ring plane, the average energy of the scattered ions in the rotating frame is comparable to the initial gyro-energy,  $E_p$  (Fig. 2). This is remarkably consistent with the measured ion temperatures (Tokar et al., 2005). However, energies larger than the initial pick up energy,  $E_p$ , and pitch angles very different from  $\pi/2$  occur as seen in Fig. 2. These results are independent of the relative collision speed and, hence, are independent of  $R$ . Although the focus above is on  $\text{O}_2^+$ ,  $\text{O}^+$  can also be scattered in ion-molecule collisions. Luhmann et al. (2005) simulated the ion motion in the presence of the dipole field with gravity, and included the scattering of both  $\text{O}_2^+$  and  $\text{O}^+$ .

Here we note that, ignoring centrifugal confinement, the magnetic latitude of the mirror point,  $\lambda_m$ , for an ion formed at  $\lambda$  with a pitch angle  $\alpha_p$ , can be approximated by  $\lambda_m^2 \approx \lambda^2 + (2/9) \cos^2 \alpha_p$  when  $\lambda_m$  and  $\lambda$  are small. This corresponds to an altitude for the northern mirror point,  $z_m \sim [0.04R_S + \lambda_m L R_S]$ . In regions where the scattering probability is small,  $\alpha_p$  is  $\sim \pi/2$  and  $z_m \sim 0.08R_S$  ( $\sim 5000$  km) as discussed above. On the other hand, for scattered  $\text{O}_2^+$ , the average value of  $\cos^2 \alpha_p$  in Fig. 2 is  $\sim 0.23$ . This corresponds to a mirror latitude  $\lambda_m \sim 0.22$  ra-

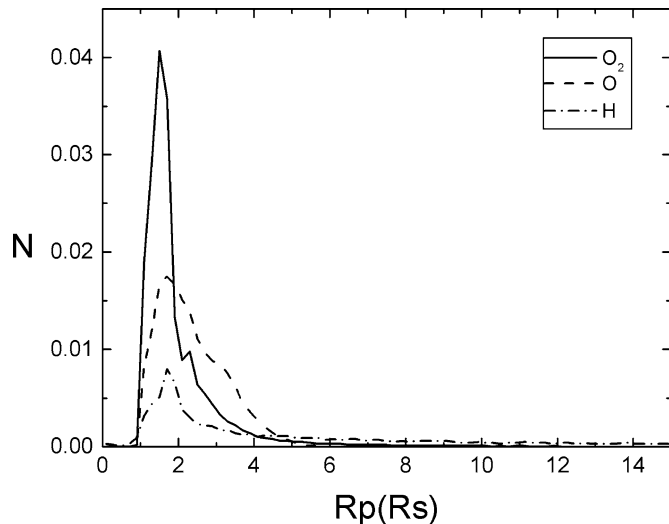


Fig. 3. Snapshot of the distribution of O (solid) and H (dashed) from dissociated  $O_2$  and  $H_2$  respectively and the distribution of  $O_2$  from  $O_2^+ + O_2$  collisions. These are formed close to the ring plane and a snap shot of the instantaneous distribution is given as a column density normalized to one vs distance  $R_p$  along the equator. The production rate over each region of the ring is proportional to the factor  $[(1-f)/(1+f)]$  in Table 2 and  $c_{ice}$  is assumed to be the same in each region. The probability of hitting the rings is proportional to  $(1-f)$ . The fractions of each of the particle populations outside the ring region ( $R > 2.27R_S$ ), including escape, for the H, O, and  $O_2$  distributions are  $\sim 0.9$ ,  $\sim 0.6$ , and  $\sim 0.4$ . The ratios are smaller than the simple model ( $\Delta E/E_o$ ) in the paper because the particles are produced close to the ring plane. Simulations are in progress to account for the differences in the vertical distribution for hydrogen and oxygen.

dians so that ions can attain altitudes well above the Cassini trajectory.

The effect of centrifugal confinement can be estimated using the ion scale height. This is written as  $H_i \sim [2kT_i/3m_i\Omega^2]^{1/2}$ , where  $T_i$  and  $m_i$  are the ion temperature and mass and  $\Omega$  is the angular velocity (Hill and Michel, 1976). Even though the velocity distribution of the scattered ions is not fully isotropic, their mean kinetic energy is close to the initial gyro energy (Fig. 2) so that  $kT_i \sim E_i^* + E_p$ , which roughly fits the measured temperatures in Fig. 1. Therefore,  $H_i$  increases as  $[\sim(1 - v_o/v_{co})R]$  for  $R$  greater than  $R_x$ , which is the equatorial radius where the Kepler orbit speed equals the co-rotation speed. To roughly account for the effect of the electrons and other ions via the electric fields Bagenal and Sullivan (1981) write  $m_i \rightarrow (m_i - m^*)$  where  $m^*$  is a function of the electron and ion temperatures and densities. Due to their frequent interaction with the ring particles, the electron temperature is small over the dense regions of the main rings. If the electron temperatures are comparable to or larger than the ion temperatures, then  $m^* \neq 0$  and the fields affect the ion motion. Assuming, initially, that  $m^* \sim 0$  then the  $H_i$  for  $O_2^+$  and  $O^+$  are  $\sim 0.18$  and  $0.22R_S$  respectively at  $R \sim 2.05R_S$ , the end of the CAPS data (Fig. 1) and go to a minimum at  $R_x$ . Since the scale heights are smaller than the average mirror altitudes estimated above over most of the measurement region, the vertical distribution of ions for  $R > R_x$  is primarily determined by centrifugal confinement consistent with simulations (Luhmann et al., 2005; Bouhram et al., 2005).

## 5. Oxygen recycling and hydrogen atmosphere

Atomic oxygen produced by photo-dissociation has an average energy  $\sim 0.8$  eV (Table 1). This is much smaller than the orbital energies near the inner edge of the C-ring and the outer edge of the A-ring [2.6 and 1.4 eV/amu, respectively]. Therefore, most of the O produced from the principal  $O_2$  loss processes returns to the surfaces of the ring particles. In addition,  $O_2^+$  and  $O^+$  can neutralize or react on these surfaces, so that atomic and molecular oxygen ions and the oxygen atoms can, *in principle*, be recycled into  $O_2$  on a ring particle surface. Although the oxygen chemistry at the surface is complex, the rate for adsorbed oxygen to be eventually recycled as  $O_2$  is controlled by the ratio of H to O in surface layers of ring particles. It has been shown, however, that this ratio is only slightly different from 2:1 for ice under irradiation (Rye et al., 1978; Brown et al., 1980). Therefore, *in steady state*, the chemical details can be ignored and the recycling of adsorbed oxygen back to  $O_2$  is determined by the relative efficiencies for the net loss of hydrogen and oxygen *from the ring/atmosphere system*.

In laboratory experiments on fresh ice samples, hydrogen is lost preferentially creating a surface which is very slightly oxygen rich, after which  $H_2$  and  $O_2$  are produced in a  $\sim 2:1$  ratio (e.g., Johnson et al., 2003). Since the energy spectrum for the desorbed  $H_2$  is close to thermal,  $H_2$  does not directly escape from the ring atmosphere. Assuming an  $H_2$  source rate twice that for  $O_2$ , densities for  $H_2$ , H,  $H_2^+$ , and  $H^+$  can also be estimated using the model above. That is, H atoms, like O, stick to the grain surfaces, whereas  $H_2$  rapidly desorbs with unit efficiency and accumulates in the atmosphere. Using only the lifetimes in Table 1, the  $H_2$  column density would be about an order of magnitude larger than that for  $O_2$  and the  $H_2^+$  column density would be comparable to that of  $O_2^+$ . However, the  $H_2$  scale height is about four times that for  $O_2$  and the relative loss rates differ. Because of the long lifetimes for  $O_2$  and  $H_2$ , these loss rates, although small, are important.

The loss of hydrogen and oxygen to Saturn's atmosphere and to the inner magnetosphere can be roughly estimated from the average excursion distance outside the ring system. This distance is roughly given by  $\Delta R \sim [\Delta E/E_o]R$ , where  $\Delta E$  is the energy given to an atom or molecule which had an orbital energy  $E_o$ . Hydrogen is more weakly 'bound' in the ring system; that is, its  $E_o$  is smaller than that for oxygen at the same orbital radius. In addition, the average energy of H following dissociation of  $H_2$  is three times larger than that for O derived from  $O_2$  (Table 1). Therefore, the average value of  $[\Delta E/E_o]$  for hydrogen is more than an order of magnitude larger than that for oxygen at the same orbital radius. Using the mean dissociation energies, the cloud of hot H from dissociation is seen to extend farther into the magnetosphere than the cloud of hot O from dissociation of  $O_2$  (Fig. 3) leading to a higher probability of escape and loss to the outer magnetosphere. Therefore, even though  $H_2$  and  $O_2$  are initially produced stoichiometrically (2:1 ratio), steady state is achieved when the oxygen density in the ring atmosphere builds up until its loss rate becomes about half the hydrogen loss rate.

If  $c_e$  is the ratio of the loss rate for two hydrogen to the loss rate for one oxygen, we can roughly account for recycling of oxygen on the ring particle surfaces. That is, the effective lifetime for oxygen in the toroidal ring atmosphere becomes  $\tau_{\text{O}_2} \sim c_e \tau'_{\text{O}_2}$ . Based on the loss rate estimates above,  $c_e \gtrsim 10$ . This indicates that the steady state  $\text{O}_2$  and  $\text{O}_2^+$  column densities and  $\text{O}_2^+$  scattering rates are at least an order of magnitude larger than the lower bounds in Table 1. The ratio of  $\text{O}_2^+$  to  $\text{H}_2^+$  content of the ring cloud in steady state is, roughly,  $c_e$  divided by the ratio of ionization times. Therefore, the  $\text{O}_2^+$  number density over the main rings is at least an order of magnitude larger than the  $\text{H}_2^+$  number density, consistent with the non-detection of  $\text{H}_2^+$  by CAPS (Young et al., 2005; Tokar et al., 2005).

## 6. Summary and comparison to CAPS data

CAPS and INMS instruments on the Cassini spacecraft measured the ionic component of the ring atmosphere vs distance from Saturn at one altitude. Here we developed a model for the neutral and ion ring atmosphere structure consistent with those measurements. Because the energetic particle flux over the main rings is small, a molecular oxygen ring atmosphere is primarily produced by the solar UV flux. This flux is more efficiently absorbed by the ring particles than by the transient water vapor produced by impacts. Therefore, we propose that the decomposition of ice on the surfaces of the ring particles by the solar UV is primarily responsible for the ring atmosphere. Dissociation of transient water vapor (Ip, 1995) and cosmic ray and energetic magnetospheric particles (Maurice et al., 2004) will be smaller additional sources subject to the same physics and chemistry described here. Therefore, the available data for the photo-production of  $\text{O}_2$  from ice was used to describe the production of an oxygen torus over Saturn's main rings with the ring particles surfaces are assumed to have an ice fraction  $c_{\text{ice}}$ .

Although freshly formed and ejected  $\text{O}_2$  has a non-thermal energy distribution,  $\text{O}_2$  adsorbs and desorbs from the surfaces of the ring particles many times during its lifetime. Therefore, the atmosphere is a *surface boundary layer atmosphere* (Johnson, 2002) with an average temperature determined primarily by the temperatures of the ring particles. The neutral component of the atmosphere is only weakly dependent on solar conditions and is similar above and below the ring plane with the largest column densities over the B-ring. Ion-molecule collisions and photo-dissociation produce a hot component, as is the case for Europa's  $\text{O}_2$  atmosphere (Shematovich et al., 2005). This acts to redistribute oxygen, which smooths the differences between the regions and populates the inner magnetosphere (e.g., Fig. 3), possibly accounting for the Cassini UV observations of oxygen (Esposito et al., 2005). As discussed, the surfaces of the ring particles, which are slightly oxidizing, can act to recycle the oxygen atoms and ions produced by photo-dissociation and ionization of  $\text{O}_2$ .

Molecular hydrogen is also produced (Johnson et al., 2003), but with a scale height about a factor of four larger than that of  $\text{O}_2$ . Although the  $\text{H}_2$  lifetime against ionization and dissociation is longer than that for  $\text{O}_2$ , it is also lost more efficiently.

In steady state the molecular oxygen atmosphere builds up until the loss of hydrogen and oxygen are, roughly, stoichiometric (2:1). When that is the case, the size of the escape ratio,  $c_e$ , suggests that the  $\text{H}_2^+$  column density is at least an order of magnitude smaller than the  $\text{O}_2^+$  column density, consistent with the CAPS data.

Since the neutral atmosphere peaks close to the ring plane, newly produced  $\text{O}_2^+$  ions would have northern mirror points about twice the altitude of the northern offset of the magnetic equator ( $\sim 0.08 R_S$ ). This is larger than the neutral scale height, but is much smaller than the altitude over the B-ring where CAPS detected ions. We propose here that these ions are scattered by collisions with  $\text{O}_2$ . Although the temperatures of the scattered ions do not differ significantly from the pick-up temperature (Fig. 2), the ions acquire a component of velocity along the field lines resulting in pitch angles that can differ significantly from  $\pi/2$  (see insert in Fig. 2). Therefore, the  $\text{O}_2^+$  temperature at the spacecraft altitude is reasonably well described by  $\sim (E_i^* + E_p)$  (Fig. 1b; Tokar et al., 2005).  $E_i^*$  is  $\sim 0.1$  eV due to the initial thermal energy ( $\sim 0.02$  eV) and the energy associated with being formed off the magnetic equator ( $\sim 0.08$  eV). The observed ion temperature exhibits a minimum near  $R_x$ , where the Kepler ( $v_o$ ) and corotation ( $v_{co}$ ) speeds are equal, and grows as  $\sim m(v_{co} - v_o)^2/2$  for larger and smaller  $R$ . The temperature of the  $\text{O}^+$  ions is also reasonably well described by  $\sim (E_i^* + E_p)$  (Fig. 1b; Tokar et al., 2005). Since  $E_i$  is  $\sim 0.5$  eV for  $\text{O}^+$ , pitch angles different from  $\pi/2$  occur at all  $R$ . Therefore, in the region around  $R_x$ , the measured  $\text{O}^+$  density is larger than the  $\text{O}_2^+$  density at the spacecraft altitude as seen in Fig. 1a. As  $R$  increases and altitude decreases, the measured  $\text{O}^+$  to  $\text{O}_2^+$  density ratio over the edge of the A-ring (Fig. 1a) approaches the branching ratio for ionization (Table 1), consistent with the INMS data (Waite et al., 2005). We ignore here the 'oscillations' in Fig. 1a, which could be real and, possibly, related to the ring structure.

The  $\text{O}_2^+$  density in Fig. 1a is seen to grow rapidly near  $R_x$  ( $v_o \approx v_{co}$ ). The peak occurs at an altitude  $\sim 0.23 R_S$ , requiring mirror latitudes  $\lambda_m \gtrsim 0.1$  that can be achieved by ion-molecule scattering. The ion density is seen to decrease in going from the peak density over the B-ring to over the inner edge of the A-ring even though the spacecraft altitude is slowly decreasing. This follows the trend for neutral source rate in our model, but not for the ion densities as discussed below. For  $R < R_x$  the densities in Fig. 1a are small. This is due, in part, to the higher spacecraft altitudes, but is also due to the fact the gravitational perturbation causes ions to precipitate with high efficiency into Saturn's atmosphere when  $R \gtrsim R_x$  (Luhmann et al., 2005). Below we discuss the region  $R > R_x$ .

Because the ion densities are only measured at one altitude, assumptions about their distribution with  $z$  are needed to compare to the model. Two estimates of the ion scale heights are given in Fig. 4a calculated using the ion temperatures,  $T_i$ , in Fig. 1b. Over most of the region these scale heights are smaller than the mean altitudes of the mirror points ( $\sim 0.22 R$ ) so that centrifugal confinement primarily determines the vertical distribution of the ions. Therefore, the ion *densities and column densities* at the magnetic equator can be estimated from the data

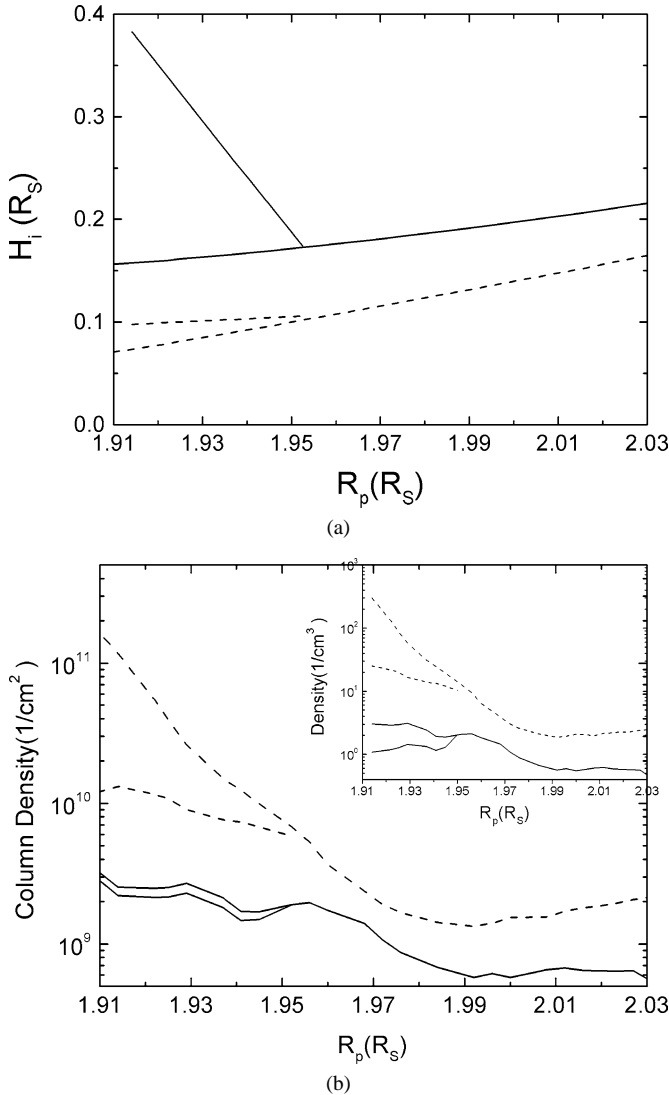


Fig. 4. (a) Estimates of centrifugal scale height,  $H_i$ , plotted vs  $R_p$  in  $R_S$  for ions  $\text{O}^+$  (solid) and  $\text{O}_2^+$  (dashed).  $H_i$  is calculated using temperatures in Fig. 1b, fit to  $kT_i \sim E_i + E_p$  (Tokar et al., 2005) and the expression  $H_i \sim [2kT_i/3(m_i - m^*)\Omega^2]^{1/2}$ . Lower estimates: assume  $m^* = 0$  (i.e., ignore ambipolar fields); upper estimates ( $m^* \neq 0$ ):  $m^*$  chosen so that the ratio of  $\text{O}_2^+$  to  $\text{O}^+$  column densities is approximately equal to the production ratio (4 to 1); column densities calculated using the measured ion density in Fig. 1a and  $H_i$ . (b) Estimates of the column density above the magnetic equator for  $\text{O}^+$  (solid) and  $\text{O}_2^+$  (dashed) vs  $R_p$  in  $R_S$ . Obtained using the scale heights in (a) and the densities in Fig. 1a. Lower curves: ( $m^* \neq 0$ ) and upper curves ( $m^* = 0$ ). Insert: corresponding ion densities at the magnetic equator.

in Fig. 1a using  $\exp[-(z/H_i)^2]$  for the variation with altitude. If we first assume that the ions act independently ( $m^* \sim 0$  in  $H_i \sim [2kT_i/3(m_i - m^*)\Omega^2]^{1/2}$ ), the lower curves in Fig. 1a are obtained. These values of the scale height determine the upper curves in Fig. 4b. It is seen that the  $\text{O}_2^+$  column density is larger than that for  $\text{O}^+$ , consistent with the photo-ionization branching ratio. However, the  $\text{O}_2^+$  column density becomes very large with decreasing  $R$  over the B-ring due to the very small values of  $H_i$

vary across the ring plane, so that a global description of the transport and loss is needed, and there can be variations in the ring particle composition affecting the O<sub>2</sub> source rate. However, the trend in going from over the B-ring through the Cassini gap to over the inner edge of the A-ring strongly suggests to us that ion transmission is occurring.

We showed that the detection of significant ion densities by Cassini at altitudes that are many times the neutral scale height is due to ion-molecule scattering. Scattering also redistributes neutral molecules (Fig. 2). Therefore, scattering and dissociation can populate the magnetosphere with H, O, H<sub>2</sub>, and O<sub>2</sub> outside of the main rings (Fig. 3). Although the photo-production rate,  $S_{O_2}$ , is small, the large surface area gives a net source  $\sim 5 \times 10^{26}$  O/s as O or O<sub>2</sub> to the region outside of the rings. The precipitation of the energetic ions onto the edge of the A-ring would add to this. The ring source rate is comparable to the total water source rate needed by Jurac and Richardson (2005) to describe the OH torus inside the orbit of Mimas ( $\sim 10^{27}$  O/s as H<sub>2</sub>O, OH, O). The redistribution of O<sub>2</sub> by ion-molecule collisions is also consistent with the CAPS detection of O<sub>2</sub><sup>+</sup> outside the edge of the A-ring (Tokar et al., 2005), a radial extension of the O<sub>2</sub> ring atmosphere (Fig. 3). Since Cassini will not pass this close to the rings again during its nominal mission, but will explore regions affected by the escape of the O<sub>2</sub> ring atmosphere, simulations of the redistribution of atoms and molecules from the ring atmosphere are in progress (e.g., Johnson et al., 2005).

The surface-bounded atmosphere of Saturn's main rings, Europa, and other icy bodies in the Solar System arise from direct exposure of cold icy bodies to the space environment. Ultraviolet photons, plasma and energetic charged particles, and micrometeoroids are ubiquitous in such environments, so similar processes are involved and lead to production of atmospheres dominated by O<sub>2</sub> cycling many times between the surface ice and atmosphere. In the planetary magnetospheres the action of co-rotating planetary fields provides energy to ions, which then scatter neutral O<sub>2</sub> into the magnetospheric environment far beyond the source region possibly contributing to the oxygen plasma near Titan (Johnson et al., 2005). Oxygen produced from ice could also be a resource for astrobiology at Europa (Cooper et al., 2001; Chyba and Hand, 2001; Johnson et al., 2003) and elsewhere, but also may provide a false positive signature for photosynthesis. Thus the new findings for Saturn's toroidal ring atmosphere need to be compared to models for Europa's atmosphere for potential application to abiotic oxygen production on extrasolar planets to be investigated by future missions such as Terrestrial Planet Finder.

## Acknowledgment

Work supported primarily by the Cassini Project under NASA/JPL contract 1243218 with SwRI. Work at the University of Virginia also supported by NASA's Planetary Atmosphere and Outer Planet Research Programs.

## References

Bagenal, F., Sullivan, J.D., 1981. Direct plasma measurements in the Io torus and the inner magnetosphere of Jupiter. *J. Geophys. Res.* 86, 8447–8466.

- Bouhram, M., Johnson, R.E., Berthelier, J.-J., Illiano, J.-M., Tokar, R.L., Young, D.T., Cray, F.J., 2005. A model of the atmosphere/ionosphere system of Saturn's main rings. *Geophys. Res. Lett.* Submitted for publication.
- Brown, W.L., Augustyniak, W.M., Brody, E., Cooper, B., Lanzerotti, J.L., Ramirez, A., Evatt, R., Johnson, R.E., 1980. Energy dependence of the erosion of H<sub>2</sub>O ice films by H and He ions. *Nucl. Instrum. Methods* 170, 321–325.
- Brown, W.L., Augustyniak, W.M., Simmons, E., Marcantonio, K.J., Lanzerotti, L.J., Johnson, R.E., Boring, J.W., Reimann, C.T., Foti, G., Pirronello, V., 1982. Erosion and molecular formation in condensed gas films by electronic energy loss of fast ions. *Nucl. Instrum. Methods B* 1, 307–314.
- Burger, M.H., Johnson, R.E., 2004. Europa's cloud: Morphology and comparison to Io. *Icarus* 171, 557–560.
- Carlson, R.W., 1980. Photosputtering of Saturn's rings. *Nature* 283, 461–462.
- Chenette, D.L., Cooper, J.F., Eraker, J.H., Pyle, K.R., Simpson, J.A., 1980. High-energy trapped radiation penetrating the rings of Saturn. *J. Geophys. Res.* 85 (A11), 5785–5792.
- Chyba, C.F., Hand, K.P., 2001. Planetary science—Life without photosynthesis. *Science* 292, 2026–2027.
- Cooper, J.F., 1983. Nuclear cascades in Saturn's rings: Cosmic ray albedo neutron decay and the origins of trapped protons in the inner magnetosphere. *J. Geophys. Res.* 88, 3945–3954.
- Cooper, J.F., Eraker, J.H., Simpson, J.A., 1985. The secondary radiation under Saturn's A–B–C rings produced by cosmic ray interactions. *J. Geophys. Res.* 90, 3415–3427.
- Cooper, J.F., Johnson, R.E., Mauk, B.H., Garrett, H.B., Gehrels, N., 2001. Energetic ion and electron irradiation of the icy Galilean satellites. *Icarus* 149, 133–159.
- Esposito, L.W., and the UVIS Team, 2005. Ultraviolet imaging spectroscopy shows an active saturnian system. *Science* 307, 1251–1256.
- Eviatar, A., McNutt Jr., R.L., Siscoe, G.L., Sullivan, J.D., 1983. Heavy ions in the outer Kronian magnetosphere. *J. Geophys. Res.* 88, 823–831.
- Grun, E., Morfill, G.E., Terrile, R.J., Johnson, T.V., Schwehm, G., 1983. The evolution of spokes in Saturn's B-ring. *Icarus* 54, 227–252.
- Hall, D.T., Strobel, D.F., Feldman, P.D., McGrath, M.A., Weaver, H.A., 1995. Detection of an oxygen atmosphere on Jupiter's moon Europa. *Nature* 373, 677–679.
- Hansen, C.J., Shemansky, D.E., Hendrix, A.R., 2005. Cassini UVIS observations of Europa's oxygen atmosphere and torus. *Icarus*. In press.
- Hill, T.W., Michel, F.C., 1976. Heavy ions from the Galilean satellites and the centrifugal distortion of the jovian magnetosphere. *J. Geophys. Res.* 81, 4561–4565.
- Huebner, W.F., Keady, J.J., Lyon, S.P., 1992. Solar photo rates for planetary atmospheres and atmospheric pollutants. *Appl. Space Sci.* 195, 1–294.
- Ip, W.-H., 1984. The ring atmosphere of Saturn: Monte Carlo simulations of the ring source model. *J. Geophys. Res.* 89, 8843–8849.
- Ip, W.-H., 1995. Exospheric systems of Saturn's rings. *Icarus* 115, 295–303.
- Ip, W.-H., 2000. Thermal plasma composition in Saturn's magnetosphere. *Planet. Space Sci.* 48, 775–783.
- Ip, W.-H., 2005. An update on the ring exosphere and plasma disc of Saturn. *Geophys. Res. Lett.* 32, doi:10.1029/2004GL022217. L13204.
- Johnson, R.E., 1990. *Energetic Charged Particle Interaction with Atmospheres and Surfaces*. Springer-Verlag, New York.
- Johnson, R.E., 2002. Surface boundary layer atmospheres. In: Mendillo, M., Nagy, A., Waite, J.H. (Eds.), *Atmospheres in the Solar System: Comparative Aeronomy Geophysical Monograph*, vol. 130. Amer. Geophys. Union, Washington, DC, pp. 203–219.
- Johnson, R.E., Quickenden, T.I., 1997. Photolysis and radiolysis of water ice on outer Solar System bodies. *J. Geophys. Res.* 102, 10985–10996.
- Johnson, R.E., Lanzerotti, L.J., Brown, W.L., 1982. Planetary applications of condensed gas sputtering. *Nucl. Instrum. Methods* 198, 147–157.
- Johnson, R.E., Quickenden, T.I., Cooper, P.D., McKinley, A.J., Freeman, C., 2003. The production of oxidants in Europa's surface. *Astrobiology* 3, 823–850. (Note: The *G*-value for Lyman-alpha induced production of O<sub>2</sub> is a factor of ten larger than in Table 2.)
- Johnson, R.E., Carlson, R.W., Cooper, J.F., Paranicas, C., Moore, M.H., Wong, M.C., 2004. Radiation effects on the surface of the Galilean satellites. In: Bagenal, F., Dowling, T., McKinnon, W.B. (Eds.), *Jupiter: The Planet*,

- Satellites and Magnetosphere. Cambridge Univ. Press, Cambridge, pp. 485–512. Ch. 20.
- Johnson, R.E., Liu, M., Sittler, E.C., 2005. Plasma-induced clearing and redistribution of material embedded in planetary magnetospheres. *Geophys. Res. Lett.* In press.
- Jurac, S., McGrath, M.A., Johnson, R.E., Richardson, J.D., Vasyliunas, V.M., Eviatar, A., 2002. Saturn: Search for a missing water source. *Geophys. Res. Lett.* 29, 2172, 25-1–4.
- Jurac, S., Richardson, J.D., 2005. A self-consistent model of plasma and neutrals at Saturn: Neutral cloud morphology. *Icarus*. In press.
- Krimigis, S.M., the MIMI Team, 2005. Dynamics of Saturn's magnetosphere from MIMI during Cassini's orbital insertion. *Science* 307, 1270–1274.
- Luhmann, J.G., Johnson, R.E., Tokar, R.L., Cravens, T., 2005. A model of the ionosphere of Saturn's toroidal ring atmosphere. *Icarus*. Submitted for publication.
- Luna, L., McGrath, M.A., Shah, M.B., Johnson, R.E., Liu, M., Latimer, C.J., Montenegro, E.C., 2005. Dissociative charge exchange and ionization of O<sub>2</sub> by fast H<sup>+</sup> and O<sup>+</sup> ions: Energetic ion interactions in the Europa's oxygen atmosphere and neutral torus. *Astrophys. J.* In press.
- Maurice, S., Cooper, J.F., Johnson, R.E., Sittler, E.C., 2004. Sources for the radiation environment of Saturn's main rings and the Innermost Radiation Belt. AGU, Fall Meeting 2004. Abstract #P52A-03.
- McGrath, M.A., Lellouch, E., Strobel, D.F., Feldman, P.D., Johnson, R.E., 2004. Satellite Atmospheres. In: Bagenal, F., Dowling, T., McKinnon, W.B. (Eds.), *Jupiter: The Planet, Satellites & Magnetosphere*. Cambridge Univ. Press, Cambridge, pp. 457–483. Ch. 19.
- Noll, K.S., Rousch, T.L., Cruikshank, D.P., Johnson, R.E., Pendleton, Y.J., 1997. Detection of ozone on Saturn's satellites Rhea and Dione. *Nature* 388, 45–47.
- Orlando, T.M., Sieger, M.T., 2003. The role of electron-stimulated production of O<sub>2</sub> from water ice in the radiation processing of outer Solar System surfaces. *Surf. Sci.* 528, 1–7.
- Orlando, T.M., Grieves, G., 2005. Production of O<sub>2</sub> from ice by sub-band gap. In preparation.
- Paranicas, C., Cheng, A.F., Mauk, B.H., Keath, E.P., Krimigis, S.M., 1997. Evidence for a source of energetic ions at Saturn. *J. Geophys. Res.* 102, 17459–17466.
- Pospieszalska, M.K., Johnson, R.E., 1991. Micrometeorite erosion of the main rings as a source of plasma in the inner saturnian plasma torus. *Icarus* 93, 45–52.
- Rye, R.R., Madey, T.E., Houston, J.E., Holloway, P.H., 1978. Chemical-state effects in Auger electron spectroscopy. *J. Chem. Phys.* 69, 1504–1512.
- Sieger, M.T., Simpson, W.C., Orlando, T.M., 1998. Production of O<sub>2</sub> on icy satellites by electronic excitation of low-temperature water ice. *Nature* 394, 554–556.
- Simpson, J.A., Bastian, T.S., Chenette, D.L., McKibben, R.B., Pyle, K.R., 1980. The trapped radiations of Saturn and their absorption by satellites and rings. *J. Geophys. Res.* 85, 5731–5762.
- Shemansky, D.E., Hall, D.T., 1992. The distribution of atomic hydrogen in the magnetosphere of Saturn. *J. Geophys. Res.* 97, 4143–4161.
- Shematovich, V.I., Johnson, R.E., Cooper, J.F., Wong, M.C., 2005. Surface-bounded atmosphere of Europa. *Icarus* 173, 480–498.
- Smith, H.T., Johnson, R.E., Shematovich, V.I., 2004. Titan's atomic and molecular nitrogen tori. *Geophys. Res. Lett.* 31, doi:10.1029/2004GL020580.
- Tokar, R.L., and 12 colleagues, 2005. Cassini Observations of the Thermal Plasma in the Vicinity of Saturn's Main Rings and the F and G Rings. *Geophys. Res. Lett.* 32, doi:10.1029/2005GL022690. L14S04.
- Waite, J.H., Cravens, T.E., Ip, W.-H., Kasprzak, W.T., Luhmann, J.G., McNutt, R.L., Niemann, H.B., Yelle, R.V., Mueller-Wodarg, I., Ledvina, S.A., Scherer, S., 2005. Cassini ion and neutral mass spectrometer measurements of oxygen ions near Saturn's A-ring. *Science*. In press.
- Westley, M.S., Baragiola, R.A., Johnson, R.E., Barrata, G.A., 1995. Ultraviolet photodesorption from water ice. *Planet. Space Sci.* 43, 1311–1315.
- Young, D.T., and 43 colleagues, 2005. Composition and dynamics of plasma in Saturn's magnetosphere. *Science* 307, 1262–1268.
- Yung, Y.L., McElroy, M.B., 1977. Stability of an oxygen atmosphere on Ganymede. *Icarus* 30, 97–103.